

High-Temperature Oxidation Performance of 4Cr4Mo2NiMnSiV Hot Die Steel

Renheng HAN¹, Ning LI¹, Ziming BAO¹, Xinjian HU¹, Hexin ZHANG^{1,2},
Chengzhi ZHAO^{1,2*}

¹ College of Materials Science and Chemical Engineering, Harbin Engineering University, No. 145 Nantong Avenue, Harbin, Heilongjiang, 150001, China

² Key Laboratory of Superlight Materials and Surface Technology of Ministry of Education, Harbin Engineering University, No. 145 Nantong Avenue, Harbin, Heilongjiang, 150001, China

crossref <http://dx.doi.org/10.5755/j02.ms.25245>

Received 07 February 2020; accepted 29 April 2020

A new type of hot working die steel was designed by using JMatPro, and high-temperature oxidation tests were carried out in the ambient atmosphere at 600 °C and 700 °C. The heat treatment process and oxidation mechanism of the designed 4Cr4Mo2NiMnSiV steel were studied in detail. XRD, SEM and EDS were used to analyze the crystallographic phases, surface and cross-section morphologies of the oxide films. The results show that the main phases in the 4Cr4Mo2NiMnSiV steel were γ and $\alpha + \delta$. During the high-temperature oxidation, oxidation of the Fe outer layer and Cr inner layer occurred. After oxidation at 600°C, the surface oxidation layer comprised a monolayer with an uneven morphology. The surface oxide film had two layers after oxidation at 700°C. The outer oxide layer mainly contained Fe₂O₃ and Fe₃O₄, while the inner oxide layer mainly contained Cr₂O₃. The microstructure was relatively regular and had a significant effect on the protection of the metallic matrix. When oxidized, the 4Cr4Mo2NiMnSiV alloy steel easily formed protective layers, such as Cr₂O₃ and SiO₂, so that the test steel had excellent oxidation resistance at high temperatures.

Keywords: JmatPro, hot working die steel, oxidation, morphology, heat treatment process.

1. INTRODUCTION

The service conditions and performance requirements of dies and molds used in modern mechanical manufacturing have become increasingly stringent due to their high-temperature working environment [1–3]. According to data [4] about current industrial production practices, approximately 80 % of parts need to be formed by using molds, and the use of molds has penetrated all aspects of modern industry. Therefore, the role of molds cannot be ignored in the equipment manufacturing industry [5]. During the use of an insert mold, the mold has to withstand very high loads and complex multidirectional stresses. The high-temperature working environment accelerates surface oxidation. At the same time, cooling of the stamped work piece is required during the stamping process. In addition, a cooling water pipeline should be designed inside the mold, and good corrosion performance of the material is required for long-term use [6]. Therefore, fabricating molds that have strong red hardness, high-temperature heat strength, excellent hardenability, corrosion resistance and good thermal stability has become a research direction of interest [7].

At present, research results have emphasized improving hot working die steels by optimizing their alloy composition and improving their heat treatment method [8, 9]. Scholars [10] developed H series hot work die steel based on the traditional 3Cr2W8V die steel by increasing the Cr content to approximately 5% and adding a small amount of alloying elements, such as Mo and Ni. Although the H series hot die steel is commonly used worldwide, this steel series is not

suitable for a working temperature of 600 °C and has poor heat resistance. To make up for those defects, scholars have developed 5Cr4W5Mo2V steel. This steel grade has a service life that is 3 times higher than that of a traditional 3Cr2W8V steel and good heat resistance properties. Although the secondary hardening effect of the mold steel is effectively improved, the toughness of the mold steel is greatly reduced, and the production application value is lowered due to the high content of Mo and W in the composition of such a mold [12]. Therefore, it is necessary to design a new series of hot working die steels.

In this study, a new steel grade was designed by combining widely used hot work die steels, such as H13 steel and 4Cr4WMoSiV, with appropriate composition improvements. In addition, the material properties dynamics calculation software JMatPro was used to design the alloy composition of the new mold steel [13–15]. Two kinds of heat treatment processes were designed to compare the high-temperature oxidation properties of the materials with two heat treatment processes. XRD, SEM, EDS and other characterization methods were used to observe the oxidation surface and oxidation morphology of the oxide film after high-temperature oxidation.

2. MATERIALS AND METHODS

2.1. Materials

In this study, pig iron (Fe ≥ 97.79 %), electrolytic copper (Cu ≥ 99.99 %), low-carbon ferro-chromium (Cr: 71.66 %), pure nickel (Ni ≥ 99.99%), ferro-molybdenum

* Corresponding author. Tel.: +86-13895718408.
E-mail address: zhaochengzhi@hrbeu.edu.cn (C. Zhao)

(Mo: 57.67 %), vanadium iron ore (V: 40.39 %) and other raw materials. The molten steel was melted in a GW medium-frequency induction furnace, cast in a metal mold and cooled in the ambient atmospheric. After the smelting was completed, the sample was processed into a square piece with a size of $a = 15$ mm. The chemical composition analysis was carried out using a Spectro MAXx direct reading spectrometer. The chemical composition of 4Cr4Mo2NiMnSiV steel is shown in Table 1.

Table 1. Chemical compositions analysis of the 4Cr4Mo2NiMnSiV test steel (mass fraction %)

Element	Cr	Mn	Ni	Mo	Si	V	Nb	C	S	P	Fe
Content	4.00	0.60	1.00	2.30	0.40	0.60	0.08	0.40	0.002	0.001	Bal.

2.2. Methods

The test alloy 4Cr4Mo2NiMnSiV was heat treated in high temperature furnace, as is shown in Fig. 1. Sample #1 was defined as a 4Cr4Mo2NiMnSiV steel, and the heat treatment process was as follows: 950 °C for 30 min, oil quenching to 350 °C, holding in an isothermal salt bath for 3 h, oil quenching to room temperature, tempering at 300 °C, holding in an isothermal salt bath for 2 h, and then normalizing to room temperature; finally, the same heat treatment process was carried out for a secondary tempering (Fig. 1 a). Sample #2 is defined as a 4Cr4Mo2NiMnSiV steel, and the heat treatment process is as follows: 1000 °C for 30 min, oil quenching, tempering at 590 °C for 2 h, and air cooling; this was followed by the same heat treatment process for the secondary tempering (Fig. 1 b). Because # 1 test steel was isothermally quenched by salt bath, it passed through the martensite + bainite composite structure in the C curve. And finally formed the martensite + bainite composite structure. The # 2 test steel was directly cooled to room temperature by oil quenching and the cooling organization was martensite organization. The secondary tempering of the experimental steel can well reduce the residual stress of the hot work die steel and enhance the performance of the material.

In this experiment, the high-temperature oxidation performance of the test steel was tested according to GB/13303-91 "Method for Determination of Oxidation Resistance of Steel". The oxidation kinetic curve was determined by static discontinuous weighing method. The size of the sample was 15 mm × 10 mm × 2 mm, and the accuracy of the weighing balance was 1×10^{-4} g. The temperature for high temperature oxidation is selected from two temperatures of 600 °C and 700 °C. The furnace is first heated to a set oxidation temperature, and then the sample is heated at a high temperature into the furnace and heated and kept, and after 2.5 h, 5 h, 10 h, 20 h, 50 h, 100 h, 150 h, 200 h, the sample is taken out from the furnace. The mixture was cooled to room temperature in a drying chamber, and weighed with an electronic balance. Each sample was weighed three times, and the average value of three measurements was taken. After the weighing was completed, the sample was placed in a furnace to continue heating and oxidation. The X Perth Pro type multi-function X-ray diffractometer (XRD) was used to analyze the phase composition of the material. The test was performed with Cu as the target, the scanning speed was 3°/min, and the

scanning range 2θ was set to 10–110°. The surface morphology and cross-section morphology of the samples after high temperature oxidation were observed by FEI QUANTA200F scanning electron microscope, and the composition was analyzed by energy dispersive spectroscopy (EDS).

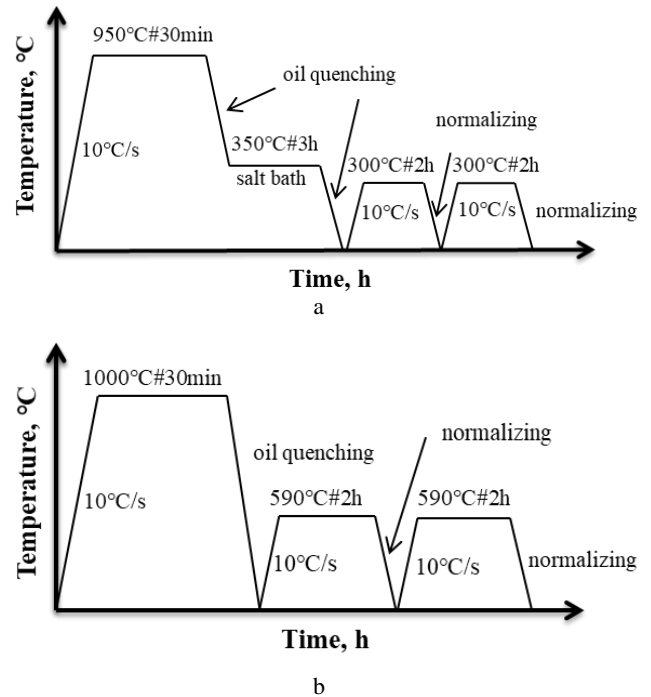


Fig. 1. Flow chart of the heat treatment process of the 4Cr4Mo2NiMnSiV test steel: a – Sample #1; b – Sample #2

3. RESULTS AND DISCUSSION

3.1. The simulated thermodynamic equilibrium phase of 4Cr4Mo2NiMnSiV

The graph in Fig. 2 shows the relationship between the phase content and temperature of 4Cr4Mo2NiMnSiV test steel determined by the JMatPro material performance simulation software.

It can be seen from the Fig. 2 that when the carbon content is set to 0.4 %, the phase composition of the alloy in the low temperature range is mainly comprised the α -Fe phase and various types of carbides (M_7C_3 , M_6C , M_2C , MC and $M_{23}C_6$). It should be pointed out that the MC-, M_2C - and M_7C_3 -type carbides can exist at 1000 °C, indicating that the above carbides are high-temperature phases. Related studies [16] have shown that MC-type carbides are mainly carbides formed by Nb, Mo and V. M_2C -type carbides are mainly formed by W and Mo. M_7C_3 is mainly a binary carbide composed of Cr, Mn, and Fe. The $M_{23}C_6$ -type carbide is mainly a binary or ternary compound composed of Cr, Mn, Fe, Mo, and W. The M_6C -type carbide is mainly a ternary carbide composed of Fe, W, and Mo. According to the composition of the alloy, the MC carbides in the alloy were mainly VC and MoC. These carbide particles were small in size, high in hardness, and dispersed in the matrix. They had a good dispersion strengthening effect and improved the high-temperature mechanical properties of the material. The M_2C -type carbides in the alloy were mainly Mo_2C , the

M_7C_3 -type carbides were mainly Cr_7C_3 and Mn_7C_3 , the $M_{23}C_6$ -type carbides were mainly $Cr_{23}C_6$ and $Mn_{23}C_6$ and the ternary carbide was $Fe_{21}Mo_2C_6$. The M_6C -type carbide was mainly a ternary carbide such as Fe_3Mo_3C , and such a carbide has good toughness. At the same time, it can be seen that the stability of the carbides in the test steel, in descending order, was $MC > M_7C_3 > M_2C > M_6C > M_{23}C_6$.

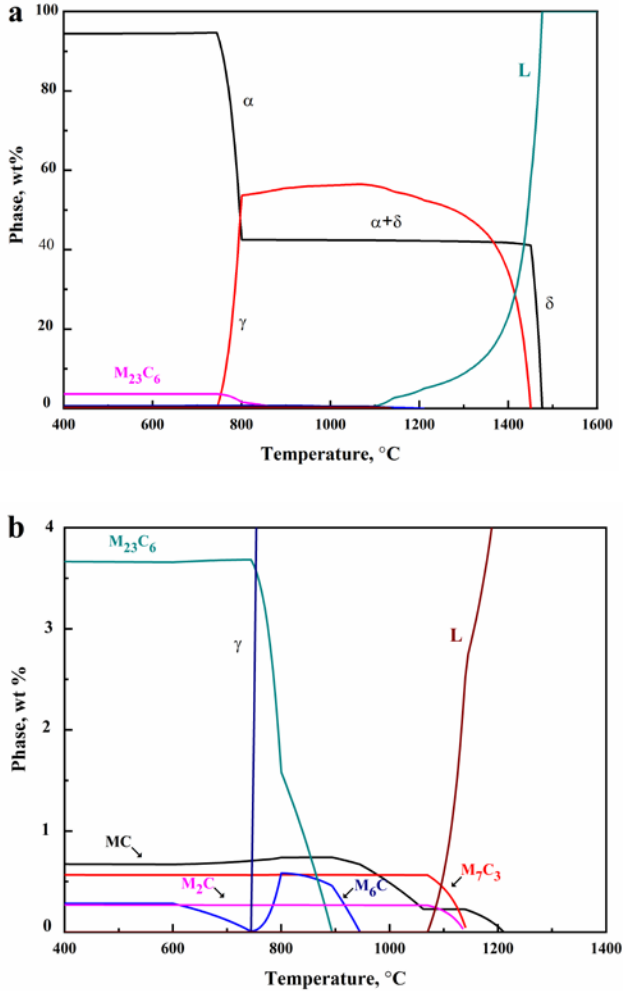


Fig. 2. The content of each phase in the 4Cr4Mo2NiMnSiV steel as a function of the temperature: a – the simulation curve; b – a partial curve

By analyzing the Fe-Fe₃C phase diagram, the melting point of the test steel was determined to be approximately 1080 °C, and the crystallization process was as follows. At 1487 °C, the homogenization transformation process occurred, and the high-temperature δ phase precipitated from the liquid phase. Subsequently, as the temperature decreased, the MC, M_7C_3 , and M_2C phases were sequentially precipitated, and their contents gradually increased with decreasing temperature and then remained unchanged. At the same time, the remaining L phase and the δ phase began to undergo a peritectic transformation to form the γ phase until the L phase completely disappeared, and the γ phase was relatively stable. Then, homologous isomerization occurred, and it did not end completely until 810 °C. At the same time, below 1000 °C, the M_6C - and $M_{23}C_6$ -type carbides began to precipitate, and as the temperature decreased, the phase content gradually increased and stabilized. At 800 °C or less, the ferrite α

phase gradually increased, and the austenite γ phase gradually decreased. At 750 °C, the austenite γ phase completely disappeared, and the α phase became stable.

3.2. Oxidation kinetics analysis

Fig. 3 presents an oxidation kinetic curve of the #1 and #2 samples at 600 °C and 700 °C in an atmospheric environment. In general, the oxidation weight gains in Fig. 3 a and b increased with time. There is no obvious increase or decrease in the figure, indicating that the oxide film did not delaminate during the oxidation process. Moreover, delamination of the oxidation film did not occur during the test process.

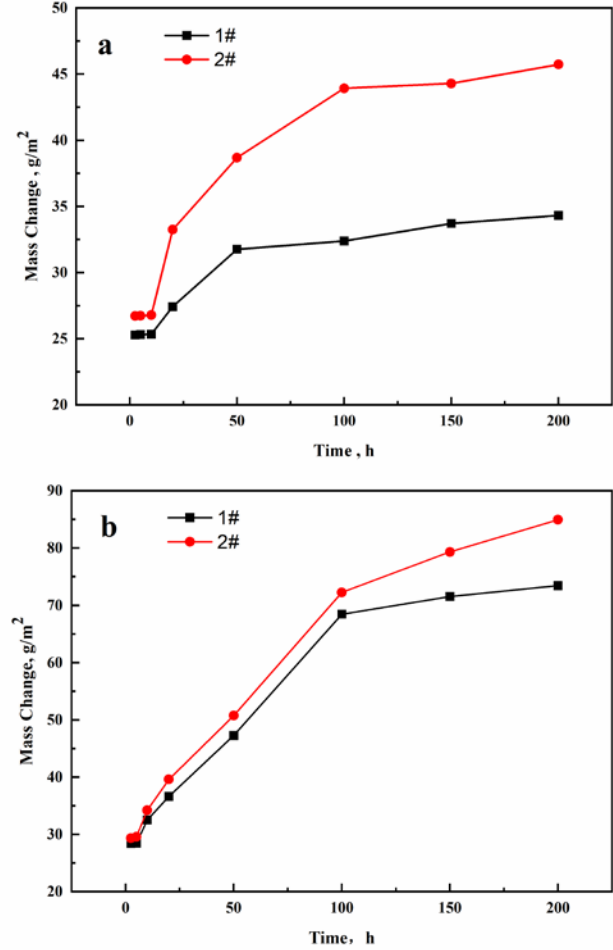


Fig. 3. Dynamic curve of high-temperature oxidation of 4Cr4Mo2NiMnSiV: a – 600 °C; b – 700 °C

The oxidation film bonded well with the substrate and tended to adhere and not delaminate. According to the calculation, the average oxidation rates of samples #1 and #2 at 600 °C were 0.171 (g/m²)/h and 0.226 (g/m²)/h, respectively. The average oxidation rates of samples #1 and #2 at 700 °C were 0.362 (g/m²)/h and 0.424 (g/m²)/h, respectively. Referring to the relevant national standards for the evaluation of the oxidation resistance of materials [17], the oxidation levels of the two samples meet the oxidation resistance level when oxidized at 600 °C and 700 °C. Overall, with increasing oxidation time, the oxidation kinetics curve of the test steel became divided into two stages: the first 100 h was the rapid oxidation stage, where the oxidation rate increased, and the last 100 h was the

stable oxidation stage, where the oxidation rate decreased.

As shown in Fig. 3 a, the oxidation kinetics curve was divided into two stages, mainly due to the different oxidation mechanisms in the high-temperature oxidation process. The O_2 ionized the metal on the surface of the air/oxide film, ions and electrons were transported through the metal oxide film and finally bonded to the oxide crystal lattice in the form of O^{2-} at the oxide layer/metallic matrix interface. At the oxidation layer/metallic matrix interface, the metal ionized to produce M^{n+} , and the metal cations migrated to the air/oxidation film through the oxidation film, which thickened the oxidation film and enabled further oxidation [18]. The oxidation process was controlled by an interfacial reaction mechanism. During the initial stage of oxidation, there was no oxidation film on the surface of the material, and the material without an oxidation film had a large contact area with the oxygen, a fast oxidation rate and selective oxidation [19, 20]. The velocity of O^{2-} in the atmosphere through the oxide film to the metal matrix was very rapid. With an extension of oxidation time, it was found that the oxidation kinetics curves of the three samples showed a plateau after 100 h. At this time, the oxidation rate was small, and the materials entered the steady oxidation stage. As the oxidation progressed, a dense oxidation film formed on the surface of the material. Further contact between the oxygen and metal matrix was prevented. Moreover, the diffusion of matrix elements was effectively prevented, and the oxidation rate decreased. On the oxidation kinetic curve, the slope of the curve decreased until a platform appeared. Since the thickness of the oxide layer was small at the start of the oxidation process, the number of electrons transported in the oxide layer was much larger than the number of ions transported. With the thickening of the oxide film, the oxide film became dense so that the oxidation rate was slowed. Fig. 3 b shows the oxidation kinetics curve at 700 °C. The general trend of the curve is basically the same as that at 600 °C. However, the oxidation rate of both samples improved relative to that at 600 °C. The increase in the temperature led to an increase in the oxidation, and the oxidation gap of the sample began to shrink, but the average oxidation rate for sample #1 was still smaller than that for sample #2. Compared with the data in Fig. 3 a, the increase in the test temperature increased the transport speed of the ions and electrons in the oxide film, and the thickness of the oxide film also increased accordingly. It can be seen that the oxidation weight gain of test steel #1 is obviously smaller than that of test steel #2; the oxidation rate is also relatively low, and the oxidation resistance improved.

3.3. XRD analysis of the oxide phase of 4Cr4Mo2NiMnSiV

Fig. 4 shows the XRD pattern of the surface oxide film from the two kinds of 4Cr4Mo2NiMnSiV steels after oxidation in an air environment for 200 h. According to Fig. 4 a, the oxide film of the experimental material was mainly composed of Fe_2O_3 and Fe_3O_4 after oxidation at 600 °C for 200 h. At the same time, the surface of sample #1 still contained the α phase, which showed better oxidation resistance than sample #2. It can be seen from Fig. 4 b that when the oxidation temperature increased, the

main component of the surface oxide of the two samples was an oxide containing Cr. When the temperature increased 700 °C, Fe_2O_3 and Fe_3O_4 appeared, and the α -Fe phase disappeared. This phenomenon indicates that the oxide film almost completely covered the substrate of the experimental material. Qualitative analysis of the oxide film thickness was based on the diffraction peak intensities in the XRD pattern [21]. The intensity of the diffraction peak from sample #2 was stronger than that from sample #1, indicating that the degree of oxidation of sample #2 was more severe. The intensity of the diffraction peaks from the #2 sample was not much different from those of the #1 sample.

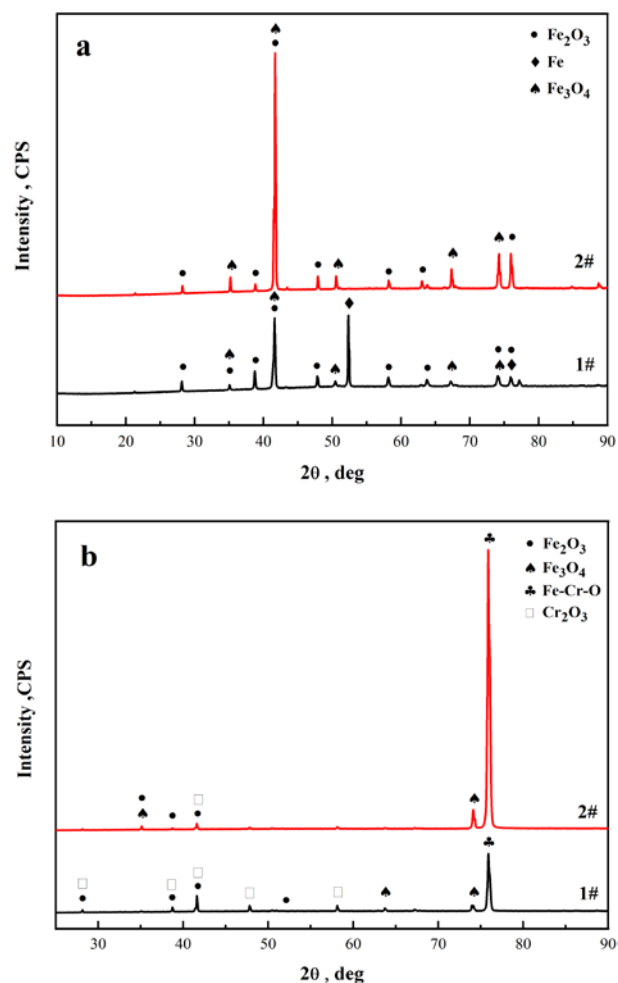


Fig. 4. XRD analysis of the oxide film on the 4Cr4Mo2NiMnSiV test steel: a – 600 °C; b – 700 °C

3.4. Analysis of the surface of the oxide film of 4Cr4Mo2NiMnSiV

To further study the oxidation mechanism of the test steel 4Cr4Mo2NiMnSiV, the microstructures of the oxidized surfaces on the two samples were observed, and the results are shown in Fig. 5. The surface morphology of the oxide film changed to varying degrees after the two samples were oxidized at the same temperature for 200 h and the same sample was oxidized at different temperatures for 200 h. As shown in Fig. 5 a and c, the microstructures of the samples of #1 and #2 were oxidized at 600 °C for 200 h. The surface oxide layer of 4Cr4Mo2NiMnSiV sample #1 contained large flaky particles. At the same time, there were

granular objects between the large flaky particles, which were stacked and overlapped to make the pores of the entire oxide layer relatively dense. The oxide film of 4Cr4Mo2NiMnSiV sample #2 was mainly composed of needle-like particles. The particle size was smaller than that of sample #1, and the particle spacing was larger than that of sample #1. A loose and fine crystalline object was distributed between the sheet-like objects. Fig. 5 b and d show the microscopic morphology of the #1 and #2 samples after oxidation at 700 °C for 200 h. Compared with the surface morphology at 600 °C, a large change occurred in the surface oxide layer of the #1 test steel, and the large pieces of flaky particles gradually disappeared and were replaced with a worm-like substance. These materials were stacked on top of each other, crossed each other and formed a grid. The dispersion of the surface pores of test steel #1 can be clearly observed so that the oxygen in the air rapidly oxidized the matrix through these pores, resulting in thickening of the oxide film. The structure of 4Cr4Mo2NiMnSiV sample #2 was replaced by a fine needle-like structure. These acicular substances were very densely distributed, and there were still a certain number of loose and fine crystalline substances between the acicular substances.

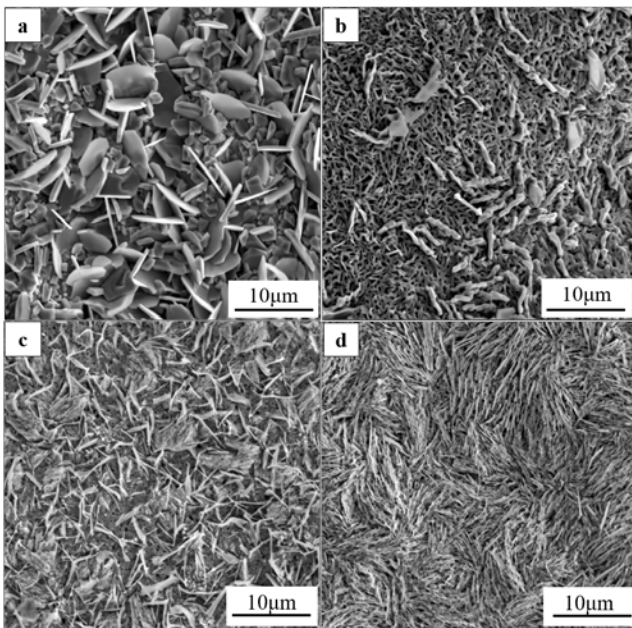


Fig. 5. SEM analysis of the surface oxide film feature of the 4Cr4Mo2NiMnSiV steel: a, b–surface morphology of sample #1/#2 oxide film at 600 °C; c, d–surface morphology of sample #1/#2 oxide film at 700 °C

Combined with the previous phase analysis and JMatPro simulation results, the main components of the 4Cr4Mo2NiMnSiV sample #1 surface at 600 °C were Fe_2O_3 and Fe_3O_4 , while the main component of the granular material was $\alpha\text{-Fe}$. When the temperature was increased 700 °C, the $\alpha\text{-Fe}$ phase disappeared, and additional Cr_2O_3 and Fe-Cr-O was produced and were mainly characterized by a staggered grid-like morphology. The main component of the worm-like morphology material was the oxide of Fe. The main components of the needle-like substance of the 4Cr4Mo2NiMnSiV sample #2 after oxidation at 700 °C were Fe_2O_3 and Fe_3O_4 , while the main component of the

loose fine crystalline substance was the oxide of Cr [22]. As the temperature increased, additional Cr in the alloy produced a large amount of the M_{23}C_6 -type carbide, which can be observed on the microscopic surface.

3.5. Cross-section analysis of oxide film of 4Cr4Mo2NiMnSiV

Fig. 6 a and b show the SEM and EDS analysis results of the #1 and #2 samples after oxidation at 600 °C for 200 h. It can be clearly seen from the SEM image of the cross section that the thickness of the oxide layer of the three samples was significantly different. According to the micron marker on the picture, it was estimated that the thickness of the oxide layer on the sample #1 steel was approximately 15–19 μm (average 15.27 μm), and the thickness of the oxide layer on the sample #2 steel was approximately 7–18 μm (average 17.59 μm).

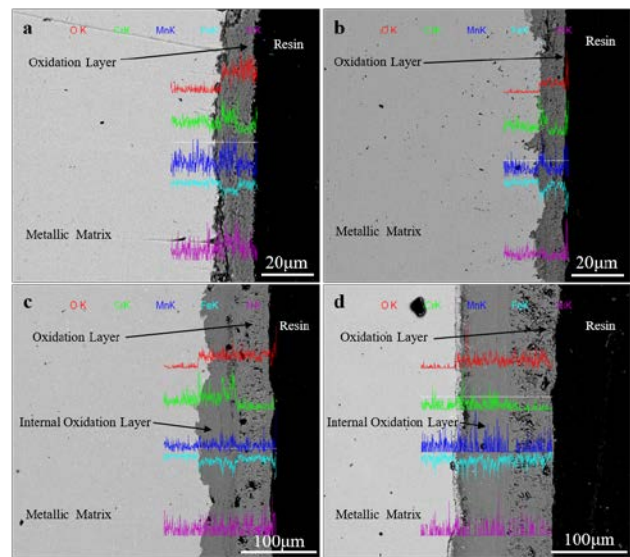


Fig. 6. SEM and EDS analysis of the oxidation cross section of 4Cr4Mo2NiMnSiV: a, b–SEM and EDS analysis of the 1#2# at 600 °C; c, d–SEM and EDS analysis of the 1#2# at 700 °C

Fig. 6 c and d show the cross-sectional morphology and EDS analysis results of three samples after oxidation at 700 °C for 200 h. The oxide layers of the two samples clearly produced different degrees of stratification, which were divided into inner and outer layers. The calculations indicated that the thickness of the oxide layer on the #1 and #2 samples was approximately 90–125 μm (average 110.59 μm) and 150–170 μm (average 156.77 μm), respectively. The oxide layer had a large degree of thickening relative to that at 600 °C. Moreover, the outer layer of the oxide film had many holes and defects, and the protection of the substrate was poor. The inner oxide film was denser and had better bonding with the metal matrix, which has good protection to the material matrix. The #1 sample produced a large number of holes at 700 °C, which is consistent with the characterization results of a large number of metal mesh structures on the surface of the oxide film.

According to the elemental analysis of the EDS line scan, the oxide film formed by the two samples experienced delamination at 700 °C. The composition of the oxide film

was mainly Fe₂O₃, which was porous and had a protective effect on the material [23]. It can be seen from Fig. 6 a and b that the thickness of the oxide layers of test steels #1 and #2 was small. The delamination of the oxide film was not obvious and was well bonded to the substrate, and cracks appeared only in certain places. It can be seen from Fig. 6 c and d that the oxide layers of test steels #1 and #2 were thick and are divided into inner and outer layers. The outer layer was porous and had large pores. According to the EDS analysis, the Fe content of the inner oxide film was lower than that of the metallic matrix and the outer oxide film. Because the iron ions continued to diffuse to the outer layer during the high-temperature process, the iron in the matrix was not easily oxidized due to the denser inner oxide layer [23]. Relative to the composition of the matrix, the Cr and Ni elements were enriched, forming a relatively dense Cr-Ni oxide layer. The high content of Cr in the alloy formed a continuous and compact Cr₂O₃ oxide film, which significantly inhibited the oxidation reaction [24]. Adding a certain amount of Si in the design of alloying elements enabled the formation of SiO₂ with a relatively stable structure in the inner oxide layer, which effectively enhanced the compactness of the Cr₂O₃ oxide film and greatly enhanced the oxidation resistance of the material [25].

4. CONCLUSIONS

The newly designed 4Cr4Mo2NiMnSiV steel mainly contained γ and $\alpha+\delta$ phases at a high temperature of 1000 °C. After different heat treatment processes, #1 test steel obtained the martensite + bainite composite structure, while #2 test steel obtained the martensite structure. The antioxidation grades of the two test steels after oxidation for 200 h at 600 °C and 700 °C met all complete antioxidant standards (< 0.1 g/m²·h). The research shows that the improved test steel increased the density of Cr₂O₃ and was beneficial to the formation of protective oxide films, such as SiO₂. The oxide film was tightly bonded to the substrate and had good anti-flaking performance. The structure of the oxide film split into two oxidation films. The outer oxide layer mainly contained Fe₂O₃ and Fe₃O₄, and the inner oxide layer mainly contained an oxide of Cr. Moreover, a protective oxide film, such as Cr₂O₃ and SiO₂, existed in the inner layer of the oxide film. It enhanced the protection of the substrate.

Acknowledgments

This research was Supported by Key Laboratory fund general projects (No. 6142905180203).

REFERENCES

- Hong, L., Zhao, C.Z., Tao, Y., Zhang, H.X. Properties of High Temperature Oxidation of Heat-resistant Steel with Aluminum and Copper *Materials Science (Medžiagotyra)* 25 (4) 2019: pp. 394–400. <https://doi.org/10.5755/j01.ms.25.4.19559>
- Han, R.H., Ning, L., Yao, H., Zhiming, L., Ziming, B., Zhao, C.Z., Zhang, H.X. Study on Wear Behaviour of 4Cr4Mo2NiMnSiV Die Steel at High Temperature *IOP Conference Series: Materials Science and Engineering* 2019: pp. 1–8.
- Li, H., Zhao, C.Z., Zhang, H.X., Wang, Q. The Influence of Cu Content on High Temperature Corrosion Behavior of Heat-Resistant Molten Salt Steel *Materials (Rio de Janeiro)* 24 (3) 2019: pp. e12455. <https://doi.org/10.1590/S1517-707620190003.0771>
- Butler, W.A. Die Casting(Permanent Mold) *Reference Module in Materials Science and Materials Engineering* 2016: pp. 70–71. <https://doi.org/10.1016/B978-0-12-803581-8.03555-4>
- Jiang, Q.C., Fang, J.R., Guan, Q.F. Thermomechanical Fatigue Behavior of Cr-Ni-Mo Cast Hot Work Die Steel *Scripta Materialia* 45 (2) 2001: pp. 199–204. [https://doi.org/10.1016/s1359-6462\(01\)01015-6](https://doi.org/10.1016/s1359-6462(01)01015-6)
- Yan, L., Keith, R., Xue, J.H., Yu, M., Duane, D., Alan, A.L. A New Fatigue Life Model for Thermally-Induced Cracking in H13 Steel Dies for Die Casting *Journal of Materials Processing Technology* 271 2019: pp. 444–454.
- Bugge, J., Sven, K., Rudolph, B. High-Efficiency Coal-Fired Power Plants Development and Perspectives *Energy* 31 (10–11) 2006: pp. 1437–1445. <https://doi.org/10.1016/j.energy.2005.05.025>
- Fang, J.R., Jiang, Q.C., Zhao, Y.G. Research and Application of Cast Hot Work Die Steel *Foundry* 51 (1) 2002: pp. 7–10.
- Abdollah, Z., Salemi, A., Assadi, H. Mechanical Behavior of CrMo Steel with Tempered Martensite and Ferrite-Bainite-Martensite Microstructure *Materials Science & Engineering A* 483–484 2008: pp. 325–328. <https://doi.org/10.1016/j.msea.2006.12.179>
- Michaud, P., Delagnes, D., Lameslea, P. The Effect of The Addition of Alloying Elements on Carbide Precipitation and Mechanical Properties in 5% Chromium Martensitic Steels *Acta Materialia* 55 (14) 2007: pp. 4877–4889. <https://doi.org/10.1016/j.actamat.2007.05.004>
- Yu, J.X., He, B.L., Li, L. The Present Situation and Development Trend of Mold Materials at Home and Abroad *Hot Working Technology* 2 (38) 2015: pp. 45–49.
- Hochanadel, P.W., Edwards, G.R., Xia-Maguire, M.C. The Effect of Microstructure on the Thermal Fatigue Resistance of Investment Cast and Wrought AISI H13 Hot Work Die Steel *Office of Scientific & Technical Information Technical Reports* 1995: pp. 1–42.
- Xie, H.J., Wu, X.C., Min, Y.G. Uniform Design and its Application in the Chemical Composition Design of Hot Work Die Steel *Key Engineering Materials* 353–358 2007: pp. 1633–1636. <https://doi.org/10.4028/www.scientific.net/KEM.353-358.1633>
- Zhang, J.G., Cong, P.W. Vacuum Heat Treatment of Hot-Work Die Steel H13 *Heat Treatment of Metals* 2005: pp. 81–84. <https://doi.org/10.4028/0-87849-963-6.77>
- Saunders, N., Guo, U.K.Z., Li, X. Using JMatPro to Model Materials Properties and Behavior *JOM* 55 (12) 2003: pp. 60–65. <https://doi.org/10.1007/s11837-003-0013-2>
- Seyed, E.V., Alireza, P., Ali, M., Mahdi, H. A Effect of Interface Strength of M₂₃C₆ in Steel Matrix on Tensile Toughness and Strength *Procedia Materials Science* 6 2007: pp. 208–215. <https://doi.org/10.1016/j.mspro.2014.07.026>
- HB5258-2000. Test Method for Determination of Oxidation Resistance of Steel and High-Temperature Alloys.

18. **Dravnieks, A., McDonald, H.J.** High Temperature Corrosion of Metals *Corrosion* 5 (7) 1949: pp. 227–233. <https://doi.org/10.5006/0010-9312-5.7.227>
19. **Ji, L., Jing, L., Wang, L.L.** Study on Carbide in Forged and Annealed H13 Hot Work Die Steel *High Temperature Materials and Processes* 34 (6) 2015: pp. 593–598. <https://doi.org/10.1515/hmp-2014-0073>
20. **Smojjan, B.** An Analysis of Relationships Between Behavior and Microstructure Constitution of Hot-Work Tool Steel *Materials & Manufacturing Processes* 24 (7–8) 2009: pp. 786–790. <https://doi.org/10.1080/10426910902813109>
21. **Shi, Q.Q., Liu, J., Yan, W.** High Temperature Oxidation Behavior of SIMP Steel and T91 Steel at 800°C *Chinese Journal of Materials Research* 2016: pp. 81–86. <https://doi.org/10.11901/1005.3093.2015.230>
22. **Zhu, L.J.** Effect of Isothermal Bainitic Treatment on Microstructure and Properties of 3Cr2MoCoWV Hot Working Die Steels *Shanghai Metals* 2011: pp. 10–13.
23. **Cheng, X.H., Wang, C.H., & Xie, Y.F.** High Temperature Mechanical and Tribological Behaviors of Hot Work Die Steel CH95 *Tribology* 23 (4) 2003: pp. 326–330.
24. **Ul, H., Mohammed, A.I. Tawancy, N.M.A.** Evolution of Oxide Scale on a Ni–Mo–Cr Alloy at 900°C *Materials Characterization* 58 (1) 2007: pp. 13–23. <https://doi.org/10.11901/j.matchar.2006.03.005>
25. **Zhao, C., Jin, T., Fu, C.** Influence of Pretreatment Process on Microstructure and Hardness of Hot-Work Die Steel 5Cr8MoNi2SiV *Heat Treatment of Metals* 2016: pp. 29–34. <https://doi.org/10.13251/j.issn.0254-6051.2016.01.006>



© Han et al. 2021 Open Access This article is distributed under the terms of the Creative Commons Attribution 4.0 International License (<http://creativecommons.org/licenses/by/4.0/>), which permits unrestricted use, distribution, and reproduction in any medium, provided you give appropriate credit to the original author(s) and the source, provide a link to the Creative Commons license, and indicate if changes were made.